Microchimica Acta (2018) 185: 399
https://doi.org/10.1007/s00604-018-2927-y

ORIGINAL PAPER

Bimetallic Pt-Pd nanostructures supported on MoS_2 as an ultra-high performance electrocatalyst for methanol oxidation and nonenzymatic determination of hydrogen peroxide

Rinky Sha[1] · Nandimalla Vishnu[1] · Sushmee Badhulika[1]

Received: 26 April 2018 / Accepted: 23 July 2018 / Published online: 2 August 2018

Abstract

The authors report on a composite based electrocatalyst for methanol oxidation and H_2O_2 sensing. The composite consists of Pt nanoparticles (NPs), Pd nanoflakes, and MoS_2. It was synthesized by chemical reduction followed by template-free electrodeposition of Pt NPs. FESEM images of the Pd nanoflakes on the MoS_2 reveal nanorod-like morphology of the Pd NPs on the MoS_2 support, whilst FESEM images of the Pt-Pd/MoS_2 composite show Pt NPs in high density and with the average size of ~15 nm, all homogeneously electrodeposited on the Pd-MoS_2 composite. A glassy carbon electrode (GCE) was modified with the composite to obtain an electrode for methanol oxidation and H_2O_2 detection. The modified GCE exhibits excellent durability with good catalytic efficiency (the ratio of forward and backward peak current density, I_f/I_b, is 3.23) for methanol oxidation in acidic medium. It was also used to sense H_2O_2 at an applied potential of −0.35 V vs. Ag|AgCl which can be detected with a 3.4 μM lower limit of detection. The sensitivity is 7.64 μA μM^{-1} cm^{-2} and the dynamic range extends from 10 to 80 μM. This enhanced performance can be explained in terms of the presence of higher percentage of metallic 1T phase rather than a semiconducting 2H phase in MoS_2. In addition, this is a result of the high surface area of MoS_2 with interwoven nanosheets, the uniform distribution of the Pt NPs without any agglomeration on MoS_2 support, and the synergistic effect of Pt NPs, Pd nanoflakes and MoS_2 nanosheets. In our perception, this binder-free nano-composite has promising applications in next generation energy conversion and in chemical sensing.

Keywords Transition metal dichalcogenides · Platinum nanoparticles · Palladium nanoflakes · Hydrothermal synthesis · Electrodeposition · Sensor

Introduction

Direct methanol fuel cells (DMFCs) have gained substantial attention as promising green power sources for electric vehicles and portable electronic devices owing to its simple fabrication procedure, low pollutant emission, high energy conversion efficiency and wide operating temperature (25–120 °C) [1–3]. Nonetheless, various technical issues such as relatively low catalytic activity, high cost and stability of electrocatalysts towards methanol electro-oxidation are still present for the commercialization of DMFCs [4, 5]. Hence, development of the economical electro-catalyst with excellent catalytic efficiency and stability is a field of research of utmost importance.

On the other hand, detection of hydrogen peroxide (H_2O_2) is of prime significance as it is extensively used as an essential mediator in environmental, pharmaceutical and food manufacturing industries [6]. The overproduction of H_2O_2 causes the progression of several diseases such as diabetes, Parkinson's, Alzheimer's, alcoholic liver disease and cancer. Electrochemical H_2O_2 sensors offer several advantages over other conventional techniques including simplicity, cost-effective, high sensitivity and faster response. Enzymatic H_2O_2 sensors use enzymes like horseradish peroxidase etc. which suffers

Rinky Sha and Nandimalla Vishnu contributed equally to this work.

Electronic supplementary material The online version of this article (https://doi.org/10.1007/s00604-018-2927-y) contains supplementary material, which is available to authorized users.

✉ Sushmee Badhulika
sbadh@iith.ac.in

[1] Department of Electrical Engineering, Indian Institute of Technology, Hyderabad 502285, India

from short-term stability and poor tolerance [6, 7]. Therefore, there is an urgent demand for developing a simple non-enzymatic H_2O_2 sensor with excellent sensitivity and selectivity.

Platinum (Pt) has been widely used as an electro-catalyst in methanol oxidation and H_2O_2 detection because of its outstanding conductivity, electro-catalytic activity and decreasing the oxidation or reduction over-potential [8–10]. However, numerous factors including high costs, poor durability and utilization efficiency, limited availability, ease of aggregation impede the widespread commercialization of Pt as an electro-catalyst [10–12]. To mitigate these issues, one of the most controlling strategies is engineering bimetallic nanostructures by alloying Pt with other less expensive metal catalyst. Palladium (Pd) is a potential co-catalyst for Pt due to its high abundance, low-cost, high stability, similar electronic structure to Pt and high catalytic activity towards electrochemical reaction [13].

Furthermore, the electro-activity, stabilization and high utilization of Pt-Pd bimetallic catalyst can be enhanced by loading catalyst onto a suitable supporting material. Over the past decade, molybdenum disulfide (MoS_2), a two dimensional, transition metal dichalcogenide (TMD), has attracted wide attention as high performance supporting material in energy storage, conversion and electrochemical sensing owing to its low-cost, layer dependent band gap, high chemical stability, ease of functionalization [14–16]. MoS_2, also known as an inorganic analogue of graphene with an exceptional structure, possesses large surface area since it comprises of Mo atoms sandwiched between two layers of hexagonal close packed sulfur atoms and this three-layer stacking held together by weak van der Waals interactions [17]. Herein, we report the bimetallic Pt-Pd nanostructures supported on MoS_2 as a multi-functional electro-catalyst wherein, Pd/MoS_2 composite was synthesized by chemical reduction method followed by template free electro-deposition of Pt nanoparticles (NPs). The Pt-Pd/MoS_2 composites were employed as electro-catalysts for methanol oxidation reaction in acidic medium and also for the detection of Hydrogen peroxide (H_2O_2) in 0.1 M phosphate buffer of pH 7. As per our knowledge, this is the first demonstration on the synthesis of Pt-Pd/MoS_2 composite and its application as an efficient, multifunctional electro-catalyst for methanol oxidation and sensing applications.

Experimental

Materials

Sodium molybdate dihydrate ($Na_2MoO_4.2H_2O$), thiourea (H_2NCSNH_2), methanol (CH_3OH), chloro-platinic acid hexahydrate (H_2PtCl_6, $6H_2O$), sodium tetra chloro-palladate (Na_2PdCl_4), sodium borohydride ($NaBH_4$), sulfuric acid (H_2SO_4), N, N-dimethyl formamide (DMF) [$(CH_3)_2NC(O)H$], hydrogen peroxide (H_2O_2), disodium phosphate (Na_2HPO_4), monosodium phosphate (NaH_2PO_4), platinum-carbon black (Pt-C black) were purchased from Sigma Aldrich (www.sigmaaldrich.com/india.html) and were used as received. Deionized (DI) water from a Millipore system (18.2 MΩ cm) was used throughout the experiments.

Electrochemical set-up

All electrochemical measurements were performed on CHI 660E electrochemical workstation at room temperature. A three electrode cell arrangement in which Pt-Pd/MoS_2 composite modified glassy carbon electrode (GCE) (3 mm in diameter) as the working electrode, Ag|AgCl electrode as the reference electrode and Pt wire as the counter electrode was employed. For methanol electro-oxidation, 0.5 M H_2SO_4 was used as the electrolyte whilst, N_2 purged 0.1 M phosphate buffer, pH 7.0 was used as the electrolyte for H_2O_2 sensing.

Synthesis of Pd-MoS_2 composite

MoS_2 was synthesized by hydrothermal route from its precursors, $Na_2MoO_4.2H_2O$ and H_2NCSNH_2. In brief, 0.3 g of $Na_2MoO_4.2H_2O$ and 0.605 g of H_2NCSNH_2 were dissolved in 30 mL DI water followed by ultrasonication for 20 min to make homogeneous solution. This solution was transferred into a 50 mL Teflon-lined stainless steel autoclave and subsequently, heated at 200 °C for 24 h. After cooling down to room temperature, the solid residue was centrifuged at 5000 rpm and washed with DI water and ethanol several times. The MoS_2 was then with dried at 70 °C in a vacuum oven overnight.

Afterwards, 15 mg of the MoS_2 was added to 15 mL of DI water and magnetically stirred for 1 h to form a stable precursor solution. 3 mg of Na_2PdCl_4 was dispersed in 1 mL DI water and then added to that of MoS_2 solution under continuous magnetic stirring. To reduce Na_2PdCl_4, here, reducing agent, $NaBH_4$ was mixed with this solution and magnetically stirred for 1 h to finish the reduction. The resulting solution was centrifuged at 10000 rpm, washed with DI water and ethanol several times and then dried at 70 °C in a hot air oven for 12 h.

Electrode fabrication

GCE was cleaned, both mechanically (polished with 0.3 and 0.05 μm alumina powder, cleaned with acetone and washed with DI water) and electrochemically (by performing 10 continuous cyclic voltammetry (CV) cycles in the potential window of −0.2 to +1.0 V vs. Ag|AgCl at a scan rate of 50 mV s^{-1} in pH 7 phosphate buffer), before each experiment and served as an underlying substrate of the working electrode. Firstly, 5 mg of Pd-MoS_2 was dissolved in 1 mL of DMF and magnetically stirred at 750 rpm for 2 h to obtain the Pd-MoS_2

stock solution. A 6 μL of this stock solution was drop-casted on the surface of the cleaned GCE and dried at 70 °C in an oven for 10 min. The Pd-MoS_2 modified GCE was then subjected to electro-deposition using amperometry technique at a potential of −0.2 V (vs. Ag| AgCl) in 0.5 M H_2SO_4 electrolytic solution containing 5 mM of $H_2PtCl_6.6H_2O$. To select the optimum Pt-Pd/MoS_2 composition for electrochemical applications, varying the electro-deposition times (450, 750 and 1000 s) of Pt on Pd-MoS_2 coated GCE were conducted. After electro-deposition, the Pt-Pd/MoS_2 modified electrodes were washed with DI water and then dried.

For electrochemical detection of H_2O_2, a stock of 20 mM H_2O_2 was prepared by adding 20.42 μL from 9.79 M H_2O_2 (30 wt.% / wt%) in 10 mL of phosphate buffer. Until further use, 9.79 M H_2O_2 and stock solutions are stored in refrigerator. For CV analyses, 500 μL of 20 mM stock was spiked in 9.5 mL of pH 7 buffer. Scan rate used during CV analyses is 50 mV s^{-1}. Likewise, the other control electrodes were tested for the electrocatalytic activity towards H_2O_2 detection. Under hydrodynamic conditions (RPM = 210), amperometric i-t experiments were performed by applying potential (E_{app}) = −0.35 V vs Ag|AgCl and spiking 5 μL of 20 mM H_2O_2 stock into 10 mL of phosphate buffer (i.e., 10 μM). Similar experiment was repeated for three electrodes ($N = 3$) and interference studies were performed at above mentioned amperometric conditions by a fresh Pt-Pd/MoS_2 electrode. For interference studies, 5 μL of 20 mM H_2O_2 stock was spiked in 10 mL of buffer and in the same pH 7 buffer 5 μL of 20 mM of glucose, 5 μL of 20 mM citric acid (CA), 5 μL of 20 mM ascorbic acid (AA) and 5 μL of 20 mM uric acid (UA) were successively spiked with at specific time intervals.

Characterization of materials

Morphology of the sample was characterized by field emission scanning electron microscope (FESEM) operated at an accelerating voltage of 5 kV. The composition of the material was determined by energy dispersive X-ray spectroscopy (EDX) attached on FE-SEM instrument. X-ray Photoelectron Spectroscopy (XPS) results were obtained using ULVAC-PHI, model no. PHI5000VersaProbeII whereas Raman spectra were recorded in the spectral range 100–600 cm^{-1} using 532 nm excitation source on Senterra, Bruker spectrometer.

Results and discussions

Characterization of Pt-Pd/MoS_2 composite

To investigate the surface morphology of the samples, FESEM analysis was performed. Fig. 1a depicts the FESEM image of MoS_2 which reveals micro-flower structure of MoS_2 containing large numbers of interwoven nanosheets. These interwoven nanosheets improve the surface area of MoS_2, consequently, offering shorter diffusion lengths for electrolytic ions and more numbers of active sites for electrochemical applications.

Fig. 1b illustrates the FESEM image of Pd-MoS_2 which reveals nanorods like morphology of Pd with high aspect ratio on the MoS_2 support. The density of Pd nanorods is not high since very low wt% of Pd precursor was used during the synthesis of Pd-MoS_2. Inset of Fig. 1b exhibits Pd nanorods with sharp and pointed edges which are not only grown on the surface of MoS_2 but also bridge the MoS_2 micro-flowers, thus demonstrating strong interactions between the MoS_2 support and Pd nanorods.

In the current work, the electro-deposition time (450, 750, 1000 s) of Pt on Pd-MoS_2 composite modified electrode was performed and systematically optimized. Fig. S1 (a) in Electronic Supplementary Material (ESM) exhibits FESEM image of Pt(450 s)-Pd/MoS_2 composite wherein Pt nanoparticles are discretely deposited on the surface of Pd-MoS_2 composite and incorporation of Pt by the electrochemical reduction of $PtCl_6^{2-}$ transforms Pd nanorods to nanoflakes like structure in nature. Fig. 1c presents FESEM image of Pt(750 s)-Pd/MoS_2 composite where high density Pt nanoparticles (NPs) with the average size of ~15 nm are homogeneously electro-deposited on Pd-MoS_2 composite. Fig. 1c further confirms the presence of Pd nanoflakes in Pt(750 s)-Pd/MoS_2 composite. This transformation of Pd nanorods to nanoflakes plays a vital role here, as it provides high surface area and large numbers of active sites for methanol electro-oxidation and sensing applications. Fig. S1(b) in ESM displays the morphology of Pt(1000s)-Pd/MoS_2 composite. With the increase in the electro-deposition time, Pt NPs become densely and agglomerate on the surface of Pd-MoS_2 composite which decreases the active sites of the electrodes.

Figure 2a presents the Raman spectrum of MoS_2. Two distinctive peaks at 381 and 408.6 cm^{-1} arise from typical E^1_{2g} and A_{1g} vibrational modes of MoS_2 respectively. The E^1_{2g} phonon mode is due to the in-plane Mo-S vibration whereas the A_{1g} mode corresponds to the out-of-plane Mo-S vibration. The peak spacing between E^1_{2g} and A_{1g} modes is directly related to the numbers of layers present in MoS_2. Here, the peak difference is 27.6 cm^{-1} indicating few layered nature (more than 4 layers) of MoS_2. In The broader and lower intensity of the E^1_{2g} peak confirms that large numbers of defects and edges are present in the MoS_2 structure [18].

Moreover, to explore the oxidation states and chemical compositions of the Pt(750 s)-Pd/MoS_2 composite, XPS analysis was performed. Fig. 2b exhibits full survey XPS spectrum of the Pt(750 s)-Pd/MoS_2 composite

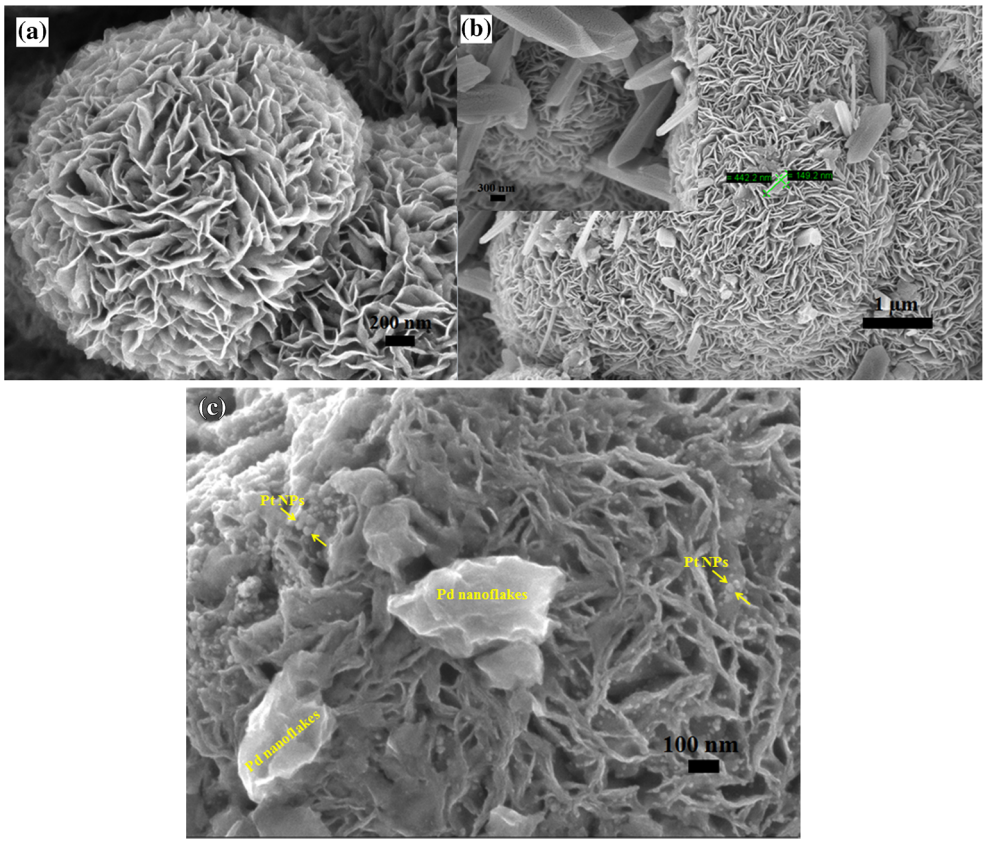

Fig. 1 FESEM images of (**a**) pure MoS_2; (**b**) Pd-MoS_2 composite at lower magnification and inset of (b): high magnification image of Pd-MoS_2 composite and (**c**) FESEM images of Pt(750 s)-Pd/MoS_2 composite

which confirms the presence of Pt, Pd and MoS_2 in the composite. Fig. 2c shows the Mo3d XPS spectrum of MoS_2 where the doublet peaks located around 228.49 eV and 231.68 eV are attributed to the $3d_{5/2}$ and $3d_{3/2}$ electronic states of Mo in Mo-S bond respectively. These two binding energies of Mo3d orbital also confirm +4 oxidation state of Mo. The Mo3d spectrum was further deconvoluted into four peaks. Two peaks at binding energy = 228.46 eV and 231.66 eV correspond to the presence of metallic 1 T phase of MoS_2 whereas other two peaks at binding energy = 229.6 eV and 233.14 eV are attributed to semiconducting 2H phase of MoS_2. Mo3d spectra revealed higher proportion of the metallic 1 T phase than the semiconducting 2H phase. Fig. 2d depicts the S2p XPS spectrum of MoS_2 wherein the peaks appeared around 162.5 eV and 163.9 eV are assigned to the $S2p_{3/2}$ and $S2p_{1/2}$ electronic states of the divalent sulfide ions respectively [19]. The Pt 4f spectrum of the Pt (750 s)-Pd/MoS_2 composite are presented in Fig. 2e which was deconvoluted into doublet peaks at binding energy = 72 eV and 75.5 eV corresponding to metallic Pt $4f_{7/2}$ and Pt $4f_{5/2}$ respectively. Doublet peaks observed at binding energy = 335.46 eV and 340.34 eV (inset Fig. 2e) are ascribed to Pd $3d_{5/2}$ and Pd 3d $_{3/2}$ orbitals respectively [20]. Detailed XPS spectra of Pt(450 s)-Pd/MoS_2 and Pt(1000s)-Pd/MoS_2 composites can be found in ESM (Fig. S2 and S3). Fig. 2f displays the EDX spectrum of Pt(750 s)-Pd/MoS_2 composite which further confirms successful formation of Pt, Pd and MoS_2 in the composite.

Electro-oxidation of methanol

The amount of Pt, electro-deposited for 450, 750 and 1000 s using amperometry technique on the Pd-MoS_2 composite modified GCE was estimated from the charge consumed during the electro-deposition of Pt using Faraday's law [21]. Based on charge consumed, the mass of Pt (m_{Pt}) for 450, 750 and 1000 s on the Pd-MoS_2 composite were found to be 12.061 µg, 19.2592 µg and 26.2502 µg respectively. With the increasing the electro-deposition time, loading of Pt on Pd-MoS_2 composite modified electrode also increases.

To assess the electro-catalytic performances of the Pt-Pd/MoS_2 composites towards methanol electro-oxidation, CV experiments were carried out in 0.5 M H_2SO_4 electrolytic solution containing 1 M methanol in the potential range of 0 to 1.1 V (vs. Ag| AgCl) at room temperature as shown in Fig. 3. Electro-oxidation of methanol yields two distinct oxidation peaks, the forward peak appeared between 0.5 and 0.9 V during the

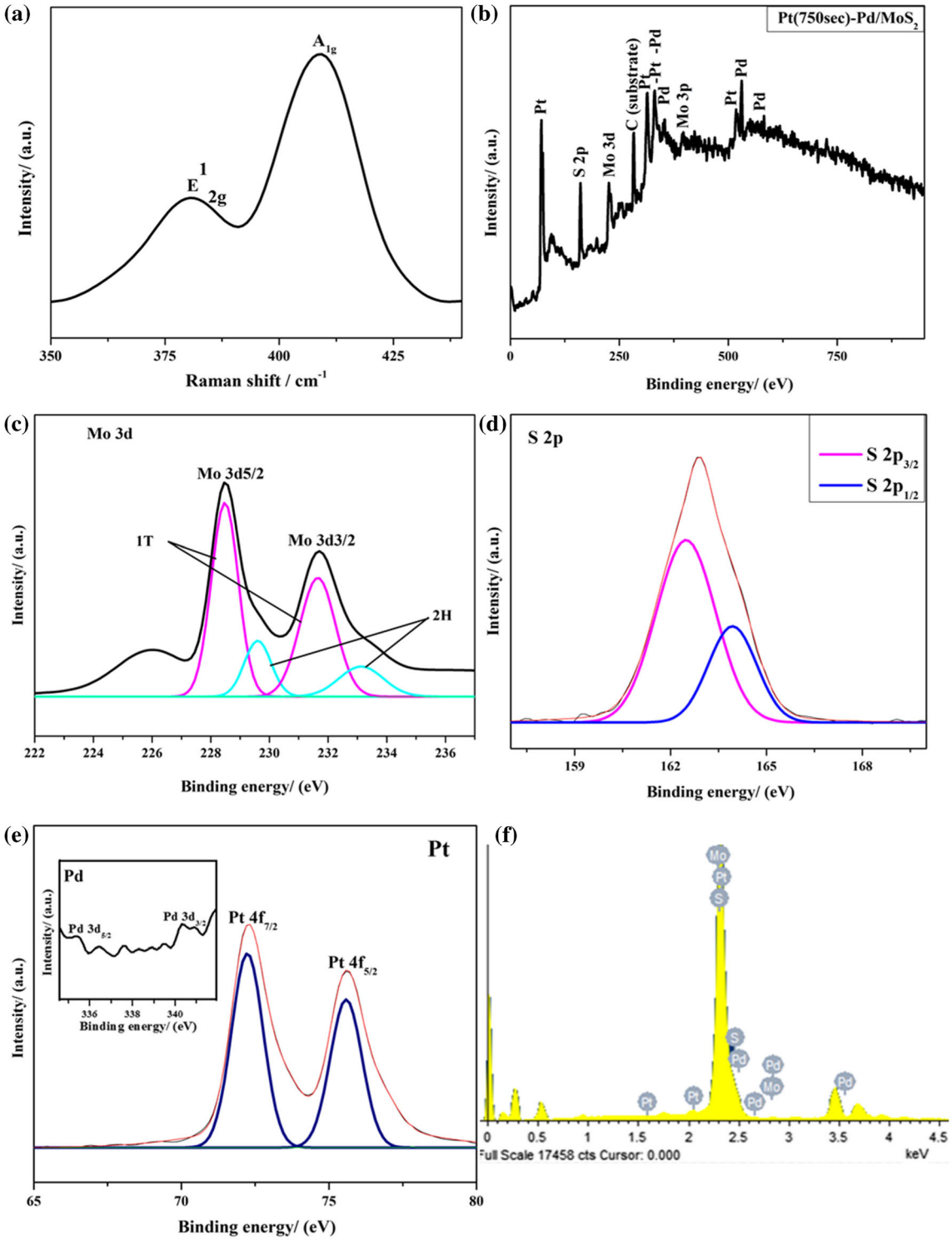

Fig. 2 **a** Raman spectrum of MoS_2; **b** XPS survey spectrum of Pt(750 s)-Pd/MoS_2 composite; **c-d** Mo3d and S2p XPS spectra of MoS_2; **e** XPS spectra of Pt and Pd (inset) and (**f**) EDX spectrum of Pt(750 s)-Pd/MoS_2 composite

forward scan while the other peak is located between 0.2 and 0.6 V in the reverse scan. The forward peak current density (I_f) corresponds to the oxidation of methanol, forming Pt-adsorbed carbonaceous intermediates such as CO which blocks the active sites of Pt, thereby preventing further oxidation of methanol as described in Eq. (1–2). Furthermore, here, Pd is used as it primarily performs the water dehydrogenation to form Pd-OH as presented in Eq. (3).

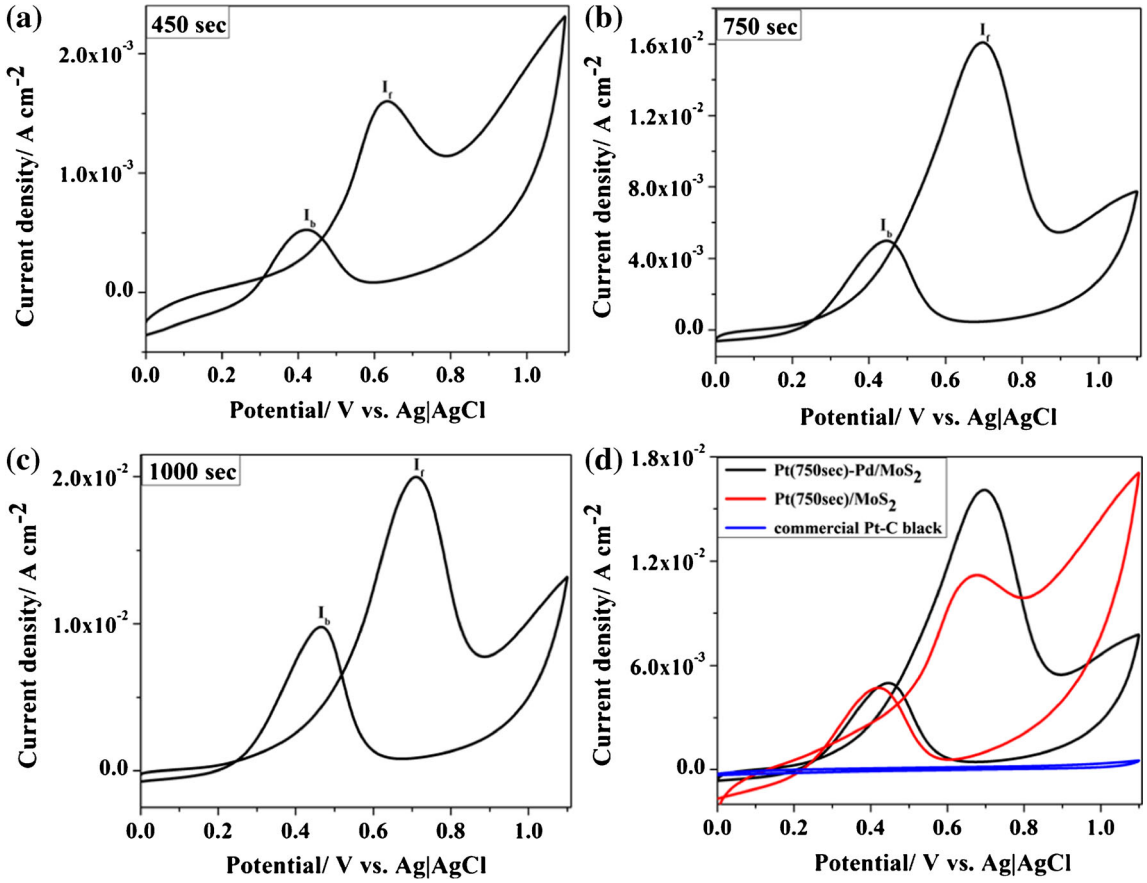

Fig. 3 CVs of (**a**) Pt(450 s)-Pd/ MoS_2, (**b**) Pt(750 s)-Pd/ MoS_2, (**c**) Pt(1000s)-Pd/ MoS_2 composites and (**d**) Comparison of Pt(750 s)-Pd/ MoS_2 and Pt(750 s)/ MoS_2 based electrodes with Pt-C black modified electrode in 0.5 M H_2SO_4 electrolytic solution containing 1 M methanol in the potential range of 0 to 1.1 V (vs. Ag| AgCl) at room temperature; scan rate: 50 mV s^{-1}

Reactions at forward peak:

$$Pt + CH_3OH \rightarrow Pt\text{-}(CH_3OH)_{ads} \quad (1)$$

$$Pt\text{-}(CH_3OH)_{ads} \rightarrow Pt\text{-}(CO)_{ads} + 4\,H^+ + 4\,e^- \quad (2)$$

$$MoS_2\text{–}Pd + H_2O \rightarrow MoS_2\text{–}Pd\,(OH)_{ads} + H^+ + e^- \quad (3)$$

The backward peak current density (I_b) is mainly ascribed to the oxidation of adsorbed carbonaceous species which are not fully oxidized during forward scan via the following bi-functional mechanism as illustrated in Eq. (4).

Reactions at backward peak:

$$Pt\text{-}(CO)_{ads} + MoS_2\text{–}Pd\,(OH)_{ads} \rightarrow Pt + MoS_2\text{–}Pd + CO_2 + H^+ + e^- \quad (4)$$

For evaluating electro-catalytic efficiency as well as catalyst's tolerance ability to intermediate carbonaceous species, I_f, I_b and the ratio of I_f/I_b are considered as important

Table 1 Comparison in the performance of Pt(750 s)-Pd/ MoS_2 composite based electrode towards MOR with other reported work

Electrode materials	C_{H2SO4}/C_{CH3OH} (M)	Scan rate (mV s^{-1})	I_f/I_b
1. PtPd/Cu_2O/rGO	0.5/0.5	50	1.47 [23]
2. Pt–MoS_2	0.5/1	50	1.44 [24]
3. PtPdCu nanodendrites	0.5/1	50	1.02 [13]
4. PtPd nanotubes	0.5/0.2	50	1.6 [25]
5. PtPd/graphene	0.5/1	50	1.709 [26]
6. PtPdPt/graphene	0.5/1	100	1.602 [27]
7. Pt(750 s)-Pd/ MoS_2	0.5/1	50	3.23 (This work)

C_{H2SO4} Concentration of sulfuric acid, C_{CH3OH} Concentration of methanol, I_f/I_b The ratio of forward and backward peak current density

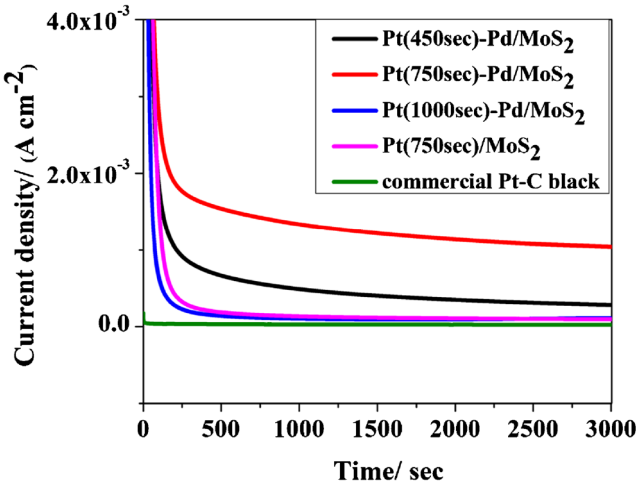

Fig. 4 Chronoamperometric responses of Pt(450, 750, 1000 s)-Pd/ MoS_2, Pt(750 s)/ MoS_2 composites and commercially available Pt-C black modified electrodes at an applied potential of +0.65 V in 0.5 M H_2SO_4 electrolytic solution containing 1 M methanol for 3000 s

indicators [22]. Preferably, an electrode with higher peak current density with larger I_f/I_b value is required for DMFC application. From Fig. 3a-c, it is clearly observed that the value of I_f increases with the increasing Pt loading on Pd-MoS_2 composite based electrode. Interestingly, among three composite nano-catalysts, Pt(750 s)-Pd/MoS_2 exhibited the highest value of I_f/I_b (3.23) which is 1.1 and 1.62 folds higher than the Pt(450 s)-Pd/MoS_2 and Pt(1000s)-Pd/MoS_2 composites respectively and also ~1.9 folds greater than other previously reported bimetallic PtPd or its composite based electrocatalysts as illustrated in Table 1 [23–27] . With the higher Pt loading, the value of I_f/I_b started decreasing demonstrating that higher Pt loading on the Pd/MoS_2 surface results in the reduction of vacant space needed for the CO liberation. The reduction of vacant space is owing to the agglomeration of high density electro-deposited Pt throughout the Pd-MoS_2 composite surface which is also evident from FESEM image of Pt(1000s)-Pd/MoS_2 (Fig. S1(b)).

Values of I_f and I_f/I_b of Pt(750 s)-Pd/MoS_2 composite (Fig. 3d) are 1.42 and 1.4 folds greater than only Pt(750 s)-MoS_2 composite respectively as in the absence of Pd, the water dehydrogenation on Pt(750 s)-MoS_2 does not occur efficiently, thus making overall methanol electro-oxidation method sluggish. Moreover, the catalytic performances of composite based electrodes are compared with commercially available Pt-C black. Pt-Pd/ MoS_2 and Pt- MoS_2 composites exhibited significant higher oxidation current responses than Pt-C black modified electrode as illustrated in Fig. 3d.

To further study the long-term stabilities of Pt-Pd/MoS_2 composites and only Pt(750 s)/MoS_2 composite, chronoamperometric responses of Pt (450, 750, 1000 s)-Pd/ MoS_2 and Pt(750 s)/ MoS_2 composites based electrodes were recorded at an applied potential of 0.65 V in 0.5 M H_2SO_4 electrolytic solution containing 1 M methanol for 3000 s as depicted in Fig. 4. Initially, the current density decreases rapidly which is ascribed to the formation of carbonaceous intermediate species, such as CO_{ads} and CHO_{ads} etc. during methanol electro-oxidation. The current density reaches at a quasi-equilibrium steady state and at 3000 s, the Pt(750 s)-Pd/ MoS_2 electrode exhibits the highest steady state current density, 1.03 mA/cm^2 which is 3.7 and 9.6 folds higher than Pt(450 s)-Pd/ MoS_2 and Pt(1000 s)-Pd/ MoS_2 based electrode. The current density of Pt(1000 s)-Pd/ MoS_2 and only Pt(750 s)/MoS_2 based electrode is almost same at 3000 s. Thus, among three electro-catalysts, the Pt(750 s)-Pd/ MoS_2 shows excellent performance in terms of stability and electro-catalytic activity. The durability of all the composite based electrodes is also compared with Pt-C black. All composites showed higher current densities at 3000 s than that of Pt-C black modified electrode.

Electrochemical sensing of H_2O_2

Prior to the H_2O_2 sensing, electrochemical impedance spectroscopic (EIS) and electrochemical surface area measurements were also carried out [28] (Fig. S4 (a & b) in ESM) and it was observed that Pt(750 s)-Pd/MoS_2 modified GCE is more suitable for electrochemical sensing applications. To probe the electrochemical behavior of the Pt(750 s)-Pd/ MoS_2 modified GCE, CV experiments were performed in the potential range of −0.4 to +0.4 V vs. Ag|AgCl in 0.1 M phosphate buffer (pH 7) in absence and presence of 1 mM H_2O_2. As illustrated in Fig. 5a, in presence of 1 mM of H_2O_2, an increase in the reduction current with the decrease in the oxidation current was observed which corresponds to the electro-catalytic reduction of H_2O_2 at the surface of Pt(750 s)-Pd/MoS_2 modified electrode.

Furthermore, to compare the electro-catalytic properties of the electrodes, GCE was modified with only MoS_2, Pd/MoS_2, Pt(750 s)/MoS_2 and Pt(750 s)-Pd/MoS_2 composite respectively. Fig. 5b depicts the electro-catalytic current responses of 1 mM H_2O_2 at the surface of bare GCE, MoS_2/GCE, Pd-MoS_2/GCE, Pt(750 s)-MoS_2/GCE and Pt(750 s)-Pd/MoS_2 modified GCE in 0.1 M phosphate buffer. The electro-catalytic current of Pt(750 s)-Pd/MoS_2 based electrode in 1 mM H_2O_2 is about 2, 4.4 and 11 folds greater than that of Pt(750 s)-MoS_2, Pd-MoS_2 and pristine MoS_2 based electrode respectively. This significant enhancement in the electro-catalytic current of the Pt(750 s)-Pd/MoS_2 composite modified electrode in H_2O_2 is attributed to the synergistic effects of MoS_2 and bimetallic nanostructures.

Amperometric measurements of different electrodes (N = 3) towards the sequential additions of H_2O_2 were carried out in the dynamic range of 10–80 μM at −0.35 V vs. Ag|AgCl in 0.1 M phosphate buffer under hydrodynamic condition. Bare GCE showed no obvious amperometric response towards

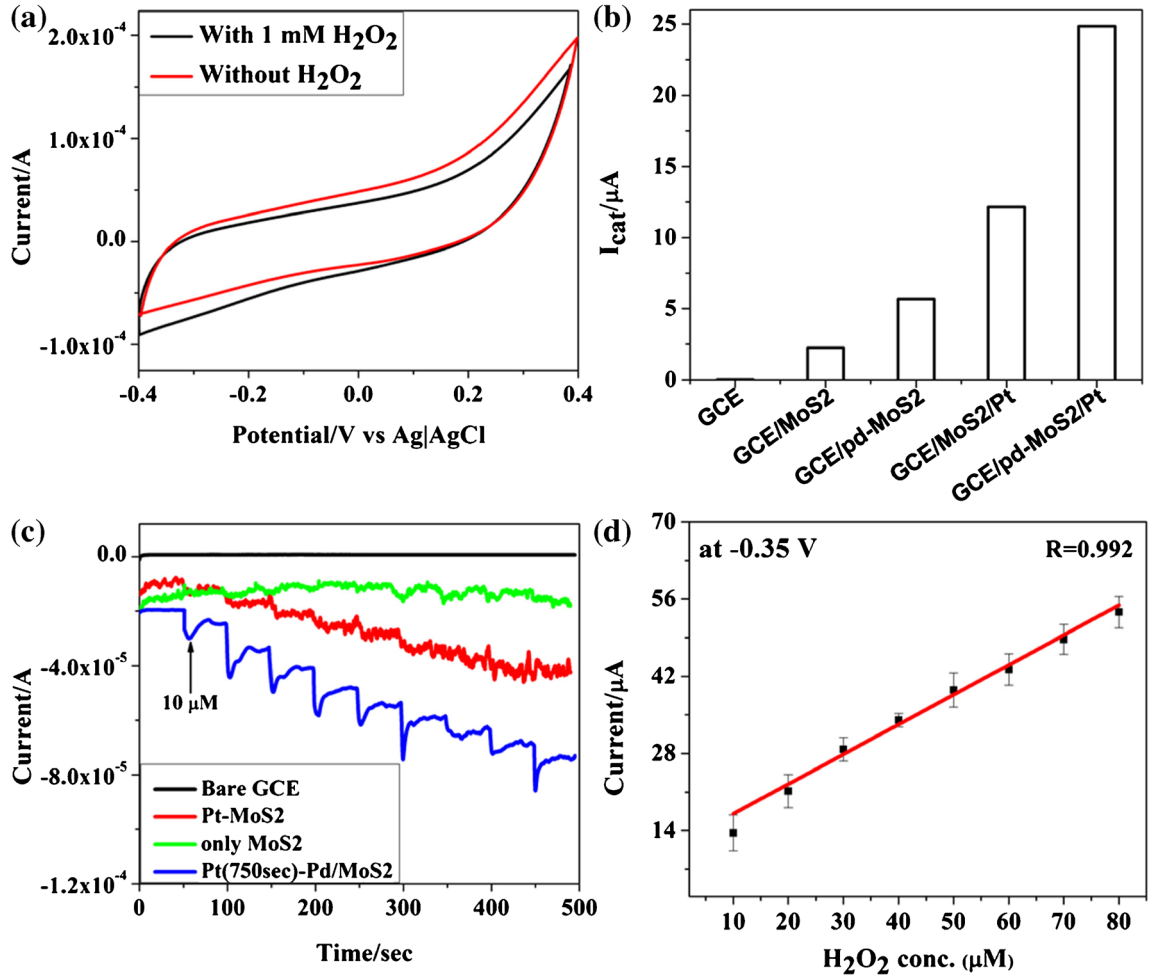

Fig. 5 **a** CVs of the Pt(750 s)-Pd/MoS_2 based sensor in a 0.1 M phosphate buffer in the absence and presence of 1 mM H_2O_2; **b** Electro-catalytic current responses of 1 mM H_2O_2 at the surface of bare GCE, MoS_2/GCE, Pd-MoS_2/GCE, Pt(750 s)-MoS_2/GCE and Pt(750 s)-Pd/MoS_2 modified GCE in 0.1 M phosphate buffer; **c** Amperometric responses of the bare GCE, MoS_2/GCE, Pt(750 s)-MoS_2/GCE and Pt(750 s)-Pd/MoS_2 modified GCE towards successive addition of H_2O_2 in the dynamic range of 10–80 μM at −0.35 V vs. Ag|AgCl in 0.1 M phosphate buffer and (**d**) Calibration curve of Pt(750 s)-Pd/MoS_2 modified GCE for different H_2O_2 concentrations (10–80 μM) for $N = 3$ electrodes

H_2O_2. Successive spike of 10 μM (Fig. 5c) of H_2O_2 results in a systematic decrease in the value of current up to 80 μM. From Fig. 5c, it is further confirmed that Pt(750 s)-Pd/MoS_2 modified GCE exhibited an enhanced amperometric response as compared to other pure MoS_2/GCE and Pt(750 s)-MoS_2/GCE towards H_2O_2 detection. The decrease in the value of current towards the sequential additions of H_2O_2 can be explicated by the following reason: H_2O_2 molecules in the 0.1 M phosphate buffer were reduced to H_2O at the electrode surface thus, decreasing the current of the Pt(750 s)-Pd/MoS_2 electrode as presented in Scheme 1.

The difference ($I_{buffer} - I_{buffer + H2O2}$) for each addition is plotted and presented in Fig. 5d. The value of correlation coefficient obtained from this calibration plot was 0.992, indicating excellent linearity of the H_2O_2 sensor. The sensitivity of the Pt(750 s)-Pd/MoS_2 based sensor was assessed using the following formula, Sensitivity = m/A, where m = the slope of calibration plot and A = surface area. The sensitivity of this sensor was found out to be 7.64 μA μM^{-1} cm^{-2}. The limit of detection (LOD) was calculated using the formula, LOD = 3S / m where, S is the standard deviation. The measured LOD was 3.4 μM which is comparatively higher than the previously reported literature [29–33]. The sensitivity of Pt(750 s)-Pd/MoS_2 modified electrode achieved was higher than other previously reported H_2O_2 sensor as shown in Table 2.

In non-enzymatic detection approach, circumventing endogenous interfering species still remains a major challenge. Hence, to investigate the selectivity of the Pt(750 s)-Pd/MoS_2 sensor, effect of other electro-active interfering species present in the physiological samples like glucose, citric acid, ascorbic acid, and uric acid was tested. Amperometric response of the Pt(750 s)-Pd/MoS_2 modified electrode was recorded at the reduction potential of −0.35 V vs. Ag|AgCl as shown in Fig. 6. First, 10 μM of H_2O_2 was spiked in 0.1 M phosphate

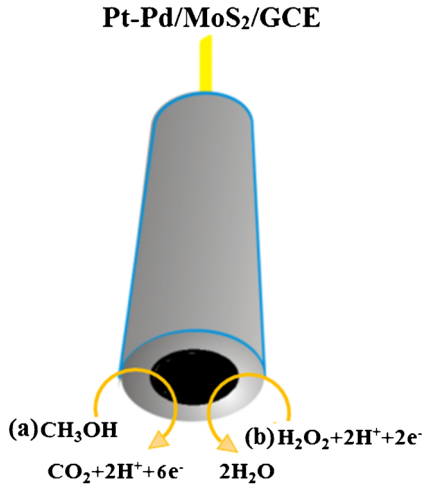

Scheme 1 Schematic demonstrating reaction mechanism of (**a**) methanol electro-oxidation and (**b**) H_2O_2 sensing at the Pt (750 s)-Pd/MoS_2 composite based electrode

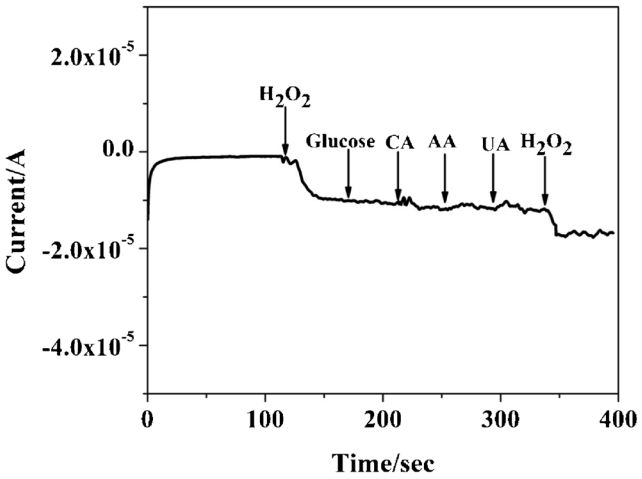

Fig. 6 Amperometric response of Pt(750 s)-Pd/MoS_2 based sensor to successive addition of 10 μM of H_2O_2 in presence of equimolar concentrations of glucose, citric acid, ascorbic acid, uric acid and at a potential of −0.35 V vs. Ag|AgCl in 0.1 M phosphate buffer

buffer. Afterwards equimolar concentration of glucose, citric acid, ascorbic acid, and uric acid was sequentially added to the electrolytic solution respectively. Nonetheless, no significant changes in the current response upon addition of interfering species were observed suggesting that the sensor has excellent selectivity towards H_2O_2 detection.

The excellent performances of Pt(750 s)-Pd/MoS_2 composite towards methanol electro-oxidation and H_2O_2 reduction can be explicated by following plausible reasons: (i) the presence of higher percentage of metallic 1 T phase than semiconducting 2H phase in MoS_2 (XPS spectrum of Pt (750 s)-Pd/MoS_2) provides higher conductivity, thus helping in achieving outstanding catalytic activities towards the methanol oxidation and H_2O_2 reduction; (ii) micro-flower structure of MoS_2, comprising of large numbers of interwoven nanosheets in the composite significantly enhances the surface area of the composite, (iii) the presence of large numbers of defects and edges in the MoS_2 structure which maps well with Raman spectrum can also act as active sites to promote direct electron transfer during the electrochemical reactions, (iv) homogeneous distribution of Pt NPs without any agglomeration on MoS_2 support in Pt(750 s)-Pd/MoS_2 composite facilitates facile penetration of the electrolytic ions inside the electrode and consequently, the electrochemical reaction between the electrolytic ions and the composite modified electrode occurs easily and (v) finally, the synergistic effect of Pt NPs, Pd nanoflakes and MoS_2 nanosheets lead to the higher conductivity and catalytic efficiency than Pt-MoS_2 composite.

There have been few reports on MoS_2 composite based catalysts for methanol electro-oxidation or H_2O_2 sensors. *Zhai* et al. [14] reported MoS_2-reduced graphene oxide composite as a support for Pt towards methanol electro-oxidation while *Xue* et al. [34] demonstrated MoS_2 NPs decorated graphene for detection of H_2O_2. Their approaches involve either high Pt loading or complex electrode fabrication techniques complex and multiple steps based synthesis techniques such as intercalation of insulating binder, nafion during electrode fabrication along with the electro-active material. But use of such binder reduces the conductivity of the electrode, thereby, reducing the catalytic efficiency and sensitivity

Table 2 Comparison in the performance of Pt(750 s)-Pd/MoS_2 composite based electrode towards H_2O_2 detection with other bimetallic and its composite based reported work

Electrode materials	pH	Eapp (V vs. Ag/AgCl)	Sensitivity (A M^{-1} cm^{-2})	LOD (μM)
1. Pt-Pd/carbon	7.4	+0.30	0.24	114 [29]
2. Pt-Pd/PDDA-rGO	7.0	0.0	0.67	0.03 [30]
3. Pt-Au/graphene-CNT	7.0	−0.55	0.31	0.6 [31]
4. Pt-W/MoS_2	7.4	−0.25	1.71	0.005 [32]
5. Pt-Ir/MWCNT	7.4	+0.25	0.05	2.5 [33]
6. Pt-Pd/MWCNT	7.4	+0.25	0.41	1.2 [33]
7. Pt(750 s)-Pd/MoS_2	7.0	−0.35	7.64	3.4 (This Work)

PDDA poly (diallyldimethylammonium chloride), *rGO* reduced graphene oxide, *Au* gold, *CNT* carbon nanotube, *W* tungsten, *Ir* iridium, *MWCNT* multiwalled CNT

towards methanol oxidation and H_2O_2 detection. In addition, this electro-catalyst offers several advantages in terms of its high catalytic efficiency, durability, excellent sensitivity with selectivity. This Pt-Pd/MoS_2 based binder-free catalyst can be used for wide electro-chemical applications.

Conclusions

In summary, a novel, efficient Pt-Pd/MoS_2 based electro-catalyst was developed for methanol electro-oxidation and sensing applications wherein Pd-MoS_2 composite prepared by chemical-reduction method followed by electro-deposition of Pt NPs. To select the optimum Pt-Pd/MoS_2 composition for electrochemical applications, an optimization study was performed by varying the electro-deposition time of Pt on Pd-MoS_2 coated GCE. FESEM image of Pd-MoS_2 composite reveals nanorods like morphology of Pd on the MoS_2 support whilst FESEM image of Pt(750 s)-Pd/MoS_2 composite exhibits high density Pt nanoparticles (NPs) with the average size of ~15 nm, uniformly electro-deposited on Pd-MoS_2 composite. Among three electro-catalysts, the Pt(750 s)-Pd/MoS_2 shows excellent performance in terms of long-term stability and electro-catalytic activity. The Pt(750 s)-Pd/MoS_2 electrode exhibited the highest value of I_f/I_b (3.23) which is also ~1.9 folds greater than other previously reported bimetallic PtPd or its composite based electro-catalysts. Furthermore, the Pt(750 s)-Pd/MoS_2 based electrode exhibited comparatively higher LOD of 3.4 μM than the previous reports with an excellent sensitivity of 7.64 μA μM^{-1} cm^{-2} towards H_2O_2 detection. This enhanced electrochemical performances were explained in terms of the presence of higher percentage of metallic 1 T phase than semiconducting 2H phase in MoS_2, high surface area because of flower-like structure of MoS_2 with interwoven nanosheets, homogeneous distribution of Pt NPs (~15 nm) without any agglomeration on MoS_2 support and the synergistic effect of Pt NPs, Pd nanoflakes and MoS_2 nanosheets. Thus, this multifunctional Pt-Pd/MoS_2 composite can be used as a potential electrode material in the field of energy storage applications and the real-time detection of H_2O_2 from cells.

Acknowledgements A part of the reported work (characterization) was carried out at the IITBNF, IITB under INUP which is sponsored by DeitY, MCIT, Government of India. The authors acknowledge the financial assistance from the Department of Science and Technology (DST), Government of India, under INSPIRE Faculty Fellowship Grant # DST/INSPIRE/04/2014/015132 and Scientific and Engineering Research Board (SERB) Young Scientist Scheme Grant # YSS/2015/000863-SERB. N.V. acknowledges Science and Engineering Research Board (SERB) National Post-Doctoral Fellowship (PDF/2017/001447) for financial support.

Compliance with ethical standards The author(s) declare that they have no competing interests.

References

1. Sha R, Badhulika S (2018) Facile synthesis of three-dimensional platinum nanoflowers on reduced graphene oxide – tin oxide composite: an ultra-high performance catalyst for methanol electro-oxidation. J Electroanal Chem 820:9–17
2. Xie J, Zhang Q, Gu L, Xu S, Wang P, Liu J, Ding Y, Yao YF, Nan C, Zhao M, You Y, Zou Z (2016) Ruthenium-platinum core–shell nanocatalysts with substantially enhanced activity and durability towards methanol oxidation. Nano Energy 21:247–257
3. Zheng J, Cullen DA, Forest RV, Wittkopf JA, Zhuang Z, Sheng W, Chen JG, Yan Y (2015) Platinum–ruthenium nanotubes and platinum–ruthenium coated copper nanowires as efficient catalysts for electro-oxidation of methanol. ACS Catal 5(3):1468–1474
4. Chen M, Meng Y, Zhou J, Diao G (2014) Platinum nanoworms self-assemble on β-cyclodextrin polymer inclusion complexes functionalized reduced graphene oxide as enhanced catalyst for direct methanol fuel cells. J Power Sources 265:110–117
5. Feng L, Li K, Chang J, Liu C, Xing W (2015) Nanostructured PtRu/C catalyst promoted by CoP as an efficient and robust anode catalyst in direct methanol fuel cells. Nano Energy 15:462–469
6. Sha R, Badhulika S (2018) Facile green synthesis of reduced graphene oxide/tin oxide composite for highly selective and ultrasensitive detection of ascorbic acid. J Electroanal Chem 816:30–37
7. Yadav MD, Dasgupta K, Kushwaha A, Srivastava AP, Patwardhan AW, Srivastava D, Joshi JB (2017) Few layered graphene by floating catalyst chemical vapour deposition and its extraordinary H_2O_2 sensing property. Mater Lett 199:180–183
8. Chen YX, Miki A, Ye S, Sakai H, Osawa M (2003) Formate, an active intermediate for direct oxidation of methanol on Pt electrode. J Am Chem Soc 125(13):3680–3681
9. Katsounaros I, Schneider WB, Meier JC, Benedikt U, Biedermann PU, Auer AA, Mayrhofer KJ (2012) Hydrogen peroxide electrochemistry on platinum: towards understanding the oxygen reduction reaction mechanism. Phys Chem Chem Phys 14(20):7384–7391
10. Zhang C, Zhang R, Gao X, Cheng C, Hou L, Li X, Chen W (2018) Small naked Pt nanoparticles confined in mesoporous shell of hollow carbon spheres for high-performance nonenzymatic sensing of H_2O_2 and glucose. ACS Omega 3(1):96–105
11. Bai Z, Dong W, Ren Y, Zhang C, Chen Q (2018) Preparation of nano au & Pt alloy microspheres decorated with reduced graphene oxide for non-enzymatic hydrogen peroxide sensing. Langmuir 34(6):2235–2244
12. Yan X, Yu S, Tang Y, Sun D, Xu L, Xue C (2018) Triangular AgAu@ Pt core–shell nanoframes with a dendritic Pt shell and enhanced electrocatalytic performance toward the methanol oxidation reaction. Nanoscale 10:2231–2235
13. Chang R, Zheng L, Wang C, Yang D, Zhang G, Sun S (2017) Synthesis of hierarchical platinum-palladium-copper nanodendrites for efficient methanol oxidation. Appl Catal B Environ 211:205–211
14. Zhai C, Zhu M, Bin D, Ren F, Wang C, Yang P, Du Y (2015) Two dimensional MoS_2/graphene composites as promising supports for Pt electrocatalysts towards methanol oxidation. J Power Sources 275:483–488
15. Lin Y, Chen X, Lin Y, Zhou Q, Tang D (2015) Non-enzymatic sensing of hydrogen peroxide using a glassy carbon electrode modified with a nanocomposite made from carbon nanotubes and molybdenum disulfide. Microchim Acta 182(9–10):1803–1809
16. Zhang W, Dai Z, Liu X, Yang J (2018) High-performance electrochemical sensing of circulating tumor DNA in peripheral blood based on poly-xanthurenic acid functionalized MoS_2 nanosheets. Biosens Bioelectron 105:116–120
17. Sun T, Li Z, Liu X, Ma L, Wang J, Yang S (2016) Facile construction of 3D graphene/MoS_2 composites as advanced electrode materials for supercapacitors. J Power Sources 331:180–188

18. Sahatiya P, Jones SS, Badhulika S (2018) Direct, large area growth of few layered MoS_2 nanostructures on different flexible substrates: growth kinetics and its effect on photodetection studies. Flex Print Electron 3:015002
19. Su S, Zhang C, Yuwen L, Liu X, Wang L, Fan C, Wang L (2016) Uniform au@Pt core–shell nanodendrites supported on molybdenum disulfide nanosheets for the methanol oxidation reaction. Nanoscale 8(1):602–608
20. Zhang Y, Chang G, Shu H, Oyama M, Liu X, He Y (2014) Synthesis of Pt–Pd bimetallic nanoparticles anchored on graphene for highly active methanol electro-oxidation. J Power Sources 262:279–285
21. Rajesh PRK, Mulchandani A (2013) Platinum nanoflowers decorated three-dimensional graphene–carbon nanotubes hybrid with enhanced electrocatalytic activity. J Power Sources 223:23–29
22. Mondal S, Malik S (2016) Easy synthesis approach of Pt-nanoparticles on polyaniline surface: an efficient electro-catalyst for methanol oxidation reaction. J Power Sources 328:271–279
23. Shahrokhian S, Rezaee S (2018) Vertically standing Cu_2O nanosheets promoted flower-like PtPd nanostructures supported on reduced graphene oxide for methanol electro-oxidation. Electrochim Acta 259:36–47
24. Patil SH, Anothumakkool B, Sathaye SD, Patil KR (2015) Architecturally designed Pt–MoS2 and Pt–graphene composites for electrocatalytic methanol oxidation. Phys Chem Chem Phys 17(39):26101–26110
25. Kim SM, Liu L, Cho SH, Jang HY, Park S (2013) Synthesis of bimetallic Pt/Pd nanotubes and their enhanced catalytic activity in methanol electrooxidation. J Mater Chem A 1:15252–15257
26. Reddy GV, Raghavendra P, Chandana PS, Sarma LS (2015) Halide-aided controlled fabrication of Pt–Pd/graphene bimetallic nanocomposites for methanol electrooxidation. RSC Adv 5:100522–100530
27. Xie W, Zhang F, Wang Z, Yang M, Xia J, Gui R, Xia Y (2016) Facile preparation of PtPdPt/graphene nanocomposites with ultrahigh electrocatalytic performance for methanol oxidation. J Electroanal Chem 761:55–61
28. Vishnu N, Gopalakrishnan A, Badhulika S (2018) Impact of intrinsic iron on electrochemical oxidation of pencil graphite and its application as supercapacitors. Electrochim Acta 269:274–281
29. Janyasupab M, Liu CW, Zhang Y, Wang KW, Liu CC (2013) Bimetallic Pt–M (M = cu, Ni, Pd, and Rh) nanoporous for H_2O_2 based amperometric biosensors. Sensors Actuators B Chem 179:2019–2214
30. Zhang Y, Zhang C, Zhang D, Ma M, Wang W, Chen Q (2016) Nano-assemblies consisting of Pd/Pt nanodendrites and poly (diallyldimethylammonium chloride)-coated reduced graphene oxide on glassy carbon electrode for hydrogen peroxide sensors. Mater Sci Eng C 58:1246–1254
31. Zhang Y, Zhang C, Zhang Y, Lin S, Wang L, Wang C (2013) Synthesis of PtAu bimetallic nanoparticles on graphene–carbon nanotube hybrid nanomaterials for nonenzymatic hydrogen peroxide sensor. Talanta 112:111–116
32. Zhu L, Zhang Y, Xu P, Wen W, Li X, Xu J (2016) PtW/MoS2 hybrid nanocomposite for electrochemical sensing of H_2O_2 released from living cells. Biosens Bioelectron 80:601–606
33. Chena KJ, Pillai KC, Rick J, Pan CJ, Wang SH, Liu CC, Hwang BJ (2012) Bimetallic PtM (M = Pd, Ir) nanoparticle decorated multiwalled carbon nanotube enzyme-free, mediator-less amperometric sensor for H_2O_2. Biosens Bioelectron 33:120–127
34. Xue Y, Maduraiveeran G, Wang M, Zheng S, Zhang Y, Jin W (2018) Hierarchical oxygen-implanted MoS_2 nanoparticle decorated graphene for the non-enzymatic electrochemical sensing of hydrogen peroxide in alkaline media. Talanta 176:397–405